Ultrasonics Sonochemistry 22 (2015) 422–428

Contents lists available at ScienceDirect

Ultrasonics Sonochemistry

journal homepage: www.elsevier.com/locate/ultson

Sonochemical-assisted synthesis of 3D graphene/nanoparticle foams and their application in supercapacitor

Kyoung G. Lee [a,1], Jae-Min Jeong [a,1], Seok Jae Lee [a], Bongjun Yeom [b], Moon-Keun Lee [a], Bong Gill Choi [c,*]

[a] Center for Nanobio Integration & Convergence Engineering (NICE), Natnioinal Nanofab Center, 291 Daehak-ro, Yuseong-gu, Daejeon 305-806, Republic of Korea
[b] Department of Chemical Engineering, University of Michigan, Ann Arbor, MI 48109, USA
[c] Department of Chemical Engineering, Kangwon National University, Samcheok 245-711, Republic of Korea

ARTICLE INFO

Article history:
Received 1 February 2014
Received in revised form 22 April 2014
Accepted 22 April 2014
Available online 2 May 2014

Keywords:
Ultrasound
3D foam
Graphene
Composite
Supercapacitor

ABSTRACT

Graphene and its derivatives have attracted much attention in application of electrochemical devices. Construction of three-dimensional (3D) heterostructured composites is promising for establishing high-performance devices, which enables large surface area, facilitated ion and electron transport, and synergistic effects between multicomponents. Here, we report a simple and general sonochemical-assisted synthesis to prepare various 3D porous graphene/nanoparticle (*i.e.*, Pt, Au, Pd, Ru, and MnO_2) foams using colloidal template. The 3D porous network structure of composite foams significantly improves a large surface area of around 550 $m^2 g^{-1}$ compared to the bare graphene (215 $m^2 g^{-1}$). This unique structure of 3D graphene/MnO_2 enables further improvement of electrochemical characteristics, compared with bare graphene/MnO_2 composite, showing a high specific capacitance of 421 $F g^{-1}$ at 0.1 $A g^{-1}$, high rate capability (97% retention at 20 $A g^{-1}$), and good cycling performance (97% retention over 1000 cycles). Moreover, electrochemical impedance analysis demonstrates that electron and ion transfer are triggered by 3D porous structure.

1. Introduction

Chemically modified graphene (CMG) materials developed by Ruoff and co-workers have shown their great potential in a wide range of applications because of their electrical, thermal, chemical, and mechanical properties [1,2]. Solution-based chemical synthesis of CMG using graphene oxide (GO) enabled mass production and facile surface functionalization [2]. Recently, all of the above merits make CMG and its derivatives attractive as nanobuilding blocks for the preparation of bulk electrodes for application of electrochemical devices [3–7]. However, these CMG-based electrodes suffer from irreversible aggregation of CMGs originating from the intersheet van der Waals force when making bulk electrode [2,8]. As a consequence, intrinsic superior features of individual CMG sheet at nanoscale cannot be transferred to the macroscopic properties of the bulk electrodes. For instance, restacking of CMG sheets causes dramatic reduction of specific surface area and inferior construction of electron and ion pathways, which are responsible for poor device performances.

Construction of three-dimensional (3D) porous structures provides a larger surface area and faster electron and ion kinetics compared to the 2D packed structures at bulk scales [9]. So far, various approaches for 3D porous frameworks have been developed, including self assembly of graphene in solution (*i.e.*, gelation and hydrothermal reduction), template-guided methods, leavening strategy, and so on [10–15]. Among them, sacrificial particle templating approaches allow us to fabricate well-defined 3D porous networks with controllable pore sizes [12,16]. Recent reports and reviews described that 3D heterogeneous structures, consisting of active nanoparticle (NP) deposited graphene sheets, are particularly promising for improving electrochemical properties of graphene-based electrodes [9,12,13,17]. However, most of previous templating methods still require a post treatment for heterogeneous structures, which is a time-consuming process and sometimes leads to the collapse of original structure.

Herein, a simple and effective approach through sonochemical synthesis was developed to prepare 3D heterogeneous CMG/NP composite foams. Polystyrene (PS) colloidal particles with size of 100 nm were employed as sacrificial templates to fabricate 3D porous structures. Ultrasound treatment was triggered simultaneously; (1) assembly of CMGs and PS spheres and (2) *in situ* synthesis of various NPs (*i.e.*, Pt, Au, Pd, Ru, and MnO_2) onto the CMG surface. Moreover, we were able to apply the 3D CMG/MnO_2 foam to

* Corresponding author. Tel.: +82 33 570 6545; fax: +82 33 570 6535.
E-mail address: bgchoi@kangwon.ac.kr (B.G. Choi).
[1] These authors contributed equally to this work.

http://dx.doi.org/10.1016/j.ultsonch.2014.04.014
1350-4177/

supercapacitor electrode, showing superior electrochemical characteristics compared to the bare CMG/MnO_2 composite.

2. Experimental

2.1. Preparation of 3D CMG/NP foams

Prior to fabricate 3D heterogeneous foams, an aqueous suspension of the negatively charged CMG sheets (10 mg) was prepared using GO suspensions by the modified Hummers method [18]. The resultant CMG solution was mixed with the positively charged PS solution in weight ratio of 95:5 wt%. At the same time, 1×10^{-3} mmol of H_2PtCl_6 was also mixed. The resultant mixture was sonicated for 15 min (Fisher Scientific Model 500 ultrasonic). During this process, pH value was maintained to be 6–8. As-synthesized CMG/PS/Pt composites were then filtered, washed with deionized (DI) water several times, and immersed in toluene to remove PS particles. The final 3D CMG/Pt foam product was rinsed with ethanol and DI water several times and dried at 60 °C under a vacuum for 24 h. Various other precursors (*i.e.*, $HAuCl_4{\cdot}3H_2O$, $Pd(C_2H_3O_2)_2$, $RuCl_3{\cdot}H_2O$, and $KMnO_4$) were used for the preparation of 3D CMG/NPs foams through the same protocol of 3D CMG/Pt foams.

2.2. Preparation of 3D CMG/MnO_2 electrode

Electrochemical properties of 3D CMG/MnO_2 foams for supercapacitor application were investigated by a conventional three-electrode electrochemical cell using 3D CMG/MnO_2-based working electrode, a KCl-Ag/AgCl of reference electrode, and a platinum wire counter electrode. The electrolyte was 1 M Na_2SO_4 solution. The working electrode was prepared by modification of Al foil substrate (1×1 cm^2) as current collector with a mixture of 3D CMG/MnO_2 (9 mg) and polytetrafluoroethylene binder (1 mg). After pressing the electrode, the electrode had bulk density of 0.86 g/cm^3. As-obtained working electrodes were dried at 60 °C under a vacuum before the performance measurements. For a reference sample, a CMG/MnO_2 electrode was prepared by the same protocol, which described the 3D CMG/MnO_2 electrode.

2.3. Characterization

Transmission electron microscopy (TEM) and high-angle annular dark-field scanning TEM (HAADF-STEM) images were collected on an E.M. 912 Ω energy-filtering TEM (JEM2200FS). Scanning electron microscopy (SEM) images were obtained using a field emission scanning electron microscope (FEI Sirion model). X-ray photoelectron spectroscopy (XPS) data were obtained using a Thermo MultiLab 2000 system with an Al Mgα X-ray source. The X-ray diffraction (XRD) data were obtained on a Rigaku D/max lllC (3 kW) with a θ/θ goniometer equipped with a CuKα radiation generator. The diffraction angle of the diffractograms was in the range of $2\theta = 5°–80°$.

2.4. Electrochemical measurements

Cyclic voltammogram was performed with a CHI 760D electrochemical workstation (CH Instruments). Galvanostatic charge/discharge measurements were carried out using a Solartron 1287A. The electrochemical impedance spectroscopy measurements were performed over a frequency range from 10^5 to 10^{-1} Hz at the amplitude of the sinusoidal voltage of 10 mV using a Solartron 1260 impedance/gain-phase analyzer. A life cycling test was taken by galvanostatic charge/discharge measurements at 1 A g^{-1} of current density up to 1000 cycles. All of the electrochemical measurements were performed at RT, and as-obtained data were within the error range of ±1%. The total capacitance C_{sp} was calculated by using the following equation:

$$C_{sp} = I/(\Delta V/\Delta t)$$

where I and $\Delta V/\Delta t$ are the applied current density and the discharge slope after *IR* drop, respectively. Upon all of the current densities (even at high current density), the discharge curves are almost linear.

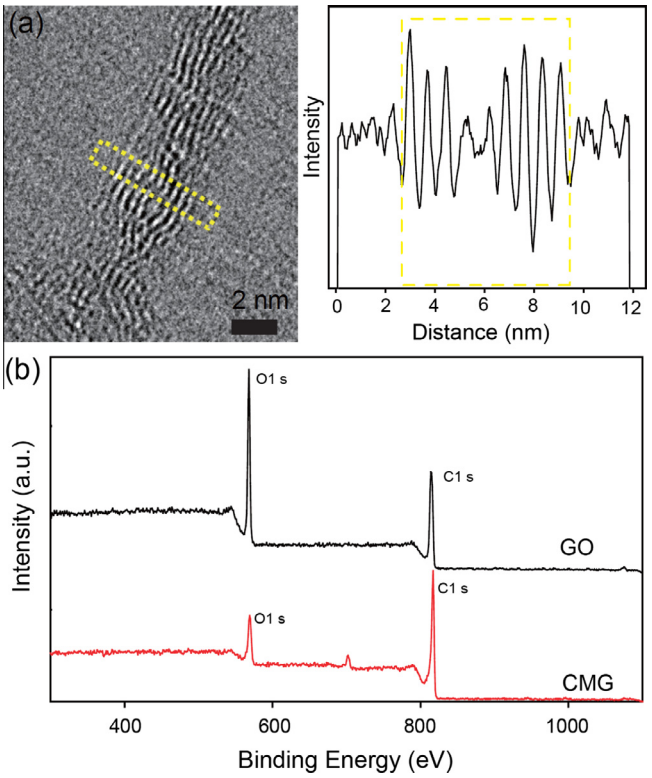

Fig. 2. (a) High-resolution TEM image of CMG sheets. (b) XPS survey spectrum of GO and CMG.

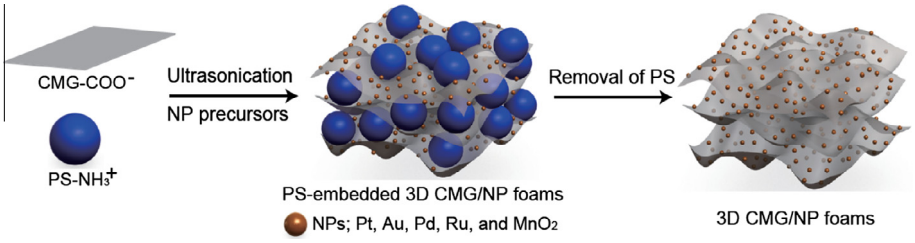

Fig. 1. Scheme of a procedure to fabricate 3D CMG/NP foams through simultaneous PS template-guided method and sonochemical synthesis.

3. Results and discussion

3D CMG/NP foams were fabricated through the sonochemical-assisted method (Fig. 1). The coassembly of the negatively charged CMGs ($CMG–COO^-$) and the positively charged PS ($PS–NH_3^+$) spheres can occur by strong electrostatic interactions under the controlled pH values of 6–8 [12,13]. The negatively charged CMGs were prepared by the modified Hummers method through controlled reduction of GOs under basic conditions [18]. As-resulted CMGs had negatively charged carboxylate groups with a few layer sheets of ~6 nm thickness (Fig. 2a). The partial oxidation of CMGs was confirmed by XPS analysis (Fig. 2b), in which the atomic ratio of C to O increases from 2.37(C = 69.23 and O = 29.17 for GO) to 5.26(C = 80.29 and O = 15.26 for CMG). Scanning electron microscopy (SEM) image of Fig. 3a shows that the PS spheres are tightly encapsulated by CMG sheets. During the electrostatic assembly, various NP precursors were *in situ* nucleated and deposited onto the surface of CMG through the ultrasound irradiation. This sonochemical approach based on acoustic cavitation is simple, fast, and effective for nucleation and growth of NPs [19,20]. After removal of PS spheres, 3D CMG/NP foams were obtained.

A typical TEM image of 3D CMG foams without NP decoration is shown in Fig. 3b. Foam-like porous structure was successfully accomplished without structural collapse. In this replicating and embossing process, electrostatic interaction between the positive charge of PS and negative charge of CMG is a critical factor for the formation of porous structures. When using negatively charged PS and non-charged PS colloids, formation of porous structures

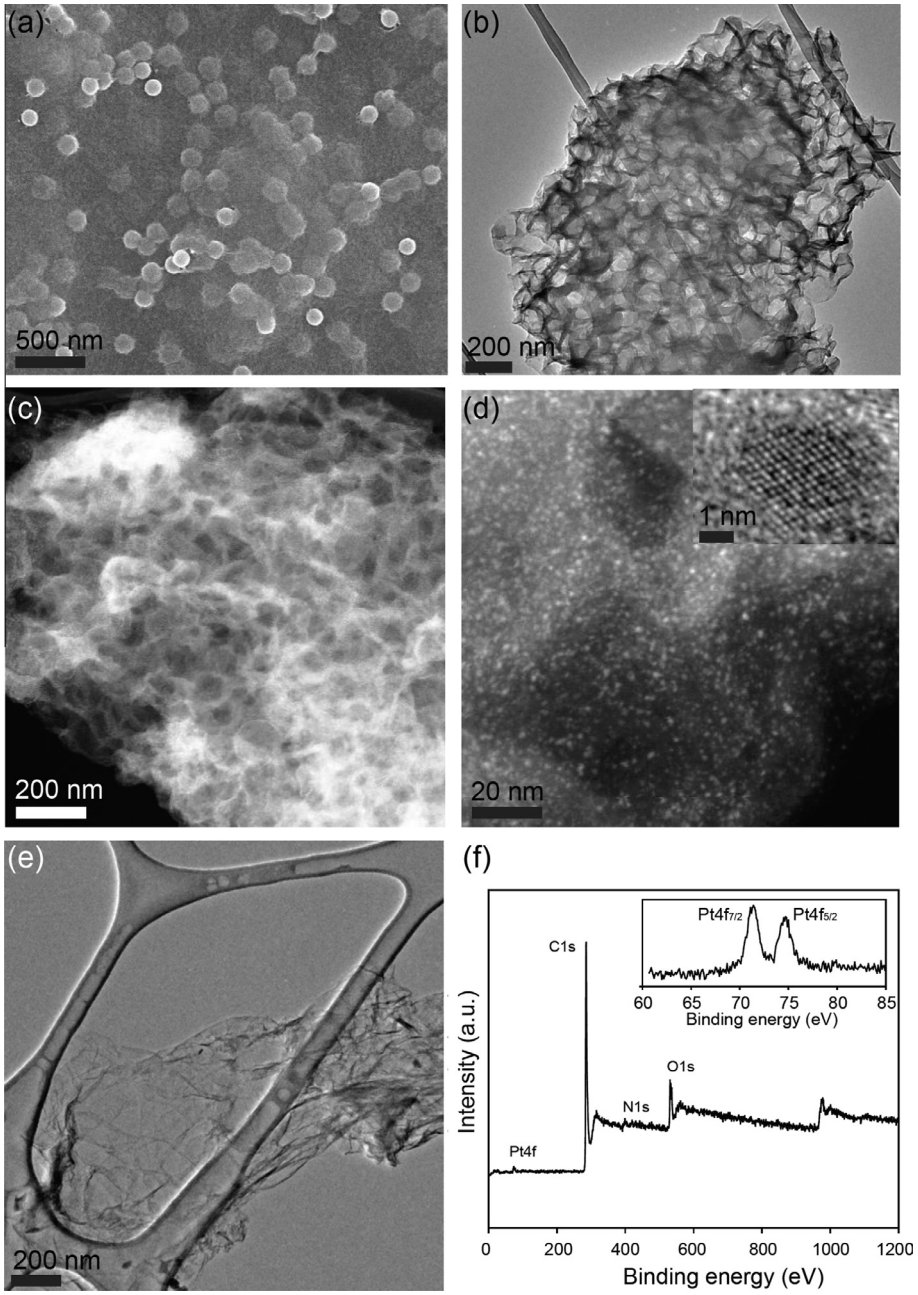

Fig. 3. (a) SEM image of PS-encapsulated CMG sheets. (b) 3D porous CMG foam after removal of PS spheres without NP precursors. (c) and (d) HAADF-STEM images of 3D CMG/Pt foams (Inset is high-resolution TEM image of a lattice structure of Pt nanoparticle onto the CMG surface.). (e) TEM image of reference sample of 3D CMG/Pt without ultrasonic treatment. (f) XPS survey spectrum of 3D CMG/Pt (Inset is Pt 4f spectrum of 3D CMG/Pt.).

were not observed due to the weak interactions between the CMG and PS. The successful embossing process enabled large surface area with porous structures. The N_2 adsorption–desorption measurement clearly demonstrated large surface area of 3D CMG (529.04 $m^2 g^{-1}$), which is 2-fold-higher than bare CMG sample (215.18 $m^2 g^{-1}$, Table 1). After deposition of Pt NPs, the 3D porous structure still remained in CMG/Pt foam (Fig. 3c). The high-angle annular dark-field scanning TEM (HAADF-STEM) images of Fig. 3c and d display that the Pt NPs were uniformly distributed on the surface of CMG sheets. High-resolution TEM measurement confirmed the lattice resolved fringes of Pt NPs, which is indicative of high crystalline structure of Pt NPs (Inset image of Fig. 3d). In contrast, deposition of Pt NPs is difficult without sonication treatment under same reaction time of CMG/Pt foam even though partial assembly of CMG and PS was observed due to the opposite surface charges of two components (Fig. 3e). Further evidence for the formation of Pt NPs was obtained from XPS analysis of 3D CMG/Pt foams (Fig. 3f).

Table 1
Textural properties of 3D CMG and 3D CMG/NPs (Pt, Ru, Pd, Au, and MnO_2) foams.

Samples	Surface area ($m^2 g^{-1}$)[a,c]	Pore volume ($cm^3 g^{-1}$)[a]	Pore size (nm)[a,b]
CMG	215.18	0.51	0.24
3D CMG	529.04	2.88	9.70
3D CMG/Pt	551.81	2.99	6.70
3D CMG/Ru	576.98	3.04	11.24
3D CMG/Pd	547.05	2.79	24.21
3D CMG/Au	560.43	3.56	17.04
3D CMG/MnO_2	559.74	3.05	8.87

[a] Properties determined with a gas sorption analyzer.
[b] Calculated by using the Barret–Joyner–Hallender (BJH) Model.
[c] Calculated by using the Brunauer–Emmett–Teller (BET) equation.

Our synthetic method provided versatility. Various types of novel NPs such as Ru, Pd, and Au were successfully synthesized on the CMG surfaces under an identical procedure to that used with the 3D CMG/Pt foam, only by changing the NP precursors. As shown in Fig. 4a–c, each sample shows successful incorporation of NPs in 3D CMG foams. In particular, metal oxide of MnO_2 was also deposited on the CMG surface through sonochemical treatment when using the $KMnO_4$ precursor. Previous reports have suggested that the redox reaction between the MnO_4^- and carbon leads to the spontaneous reduction of MnO_4^- ions to MnO_2 on the surface of CMGs [19,21]. The ultrasound irradiation facilitated the formation of MnO_2 on the surface of CMGs [21]. The formation of NPs was confirmed by each XPS analysis (Inset images of Fig. 4). Different morphologies and sizes of NPs were attributed to different types of NP precursors and growth kinetic mechanisms of NPs [22,23]. These 3D CMG/NP foams had high surface areas around 550 $m^2 g^{-1}$ (Table 1).

One promising potential to harness these 3D CMG/NP foams is an electrode material for electrochemical capacitors. MnO_2 is the most thoroughly investigated material for supercapacitors because of its high theoretical specific capacitance (1370 $F g^{-1}$) with low cost [24]. In addition, a combination of its high surface area, high electrical conductivity, and porous structures is desirable to enhance power and energy performances of supercapacitors. Hence, we selected 3D CMG/MnO_2 sample for application of

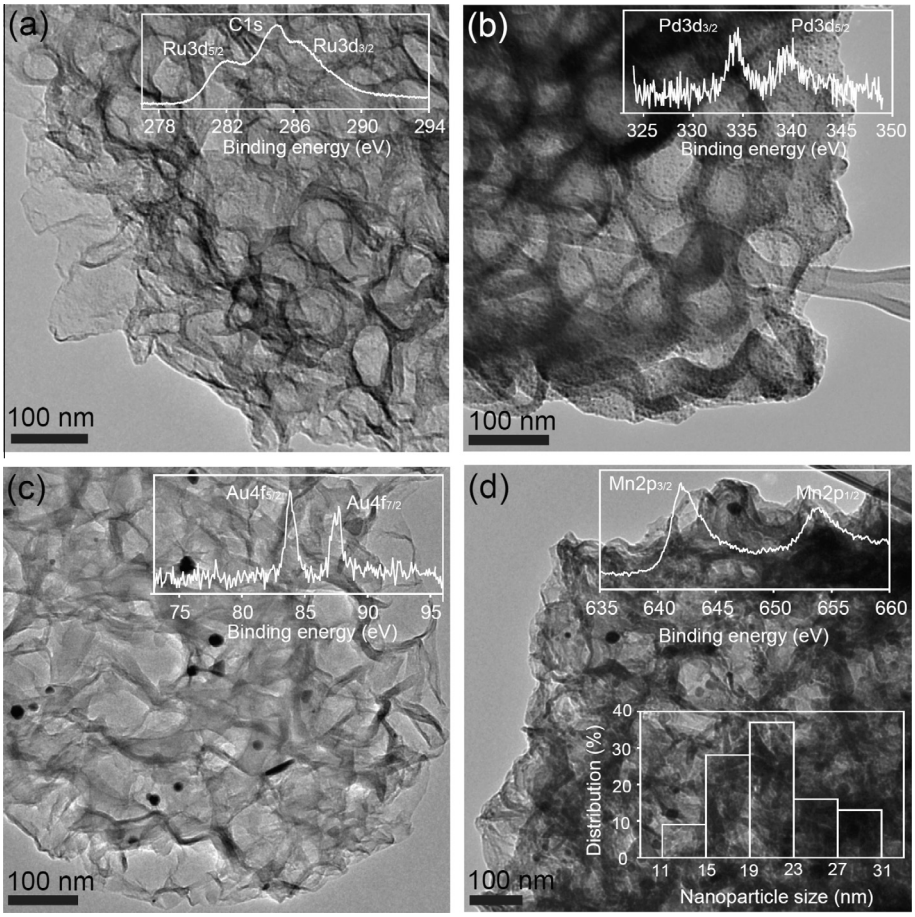

Fig. 4. TEM images and XPS spectra for (a) 3D CMG/Ru, (b) 3D CMG/Pd, (c) 3D CMG/Au, and (d) 3D CMG/MnO_2 foams. Inset of (d) is size distribution of MnO_2 particle.

supercapacitor electrode. The MnO_2 obtained from ultrasonic treatment has amorphous structure, verified by XRD patterns of Fig. 5a. In addition, when observing Mn 3s peaks, the MnO_2 exhibits a peak separation of ~4.9 eV, which is indicative of an intermediate oxidation state between Mn^{4+} and Mn^{3+} (Fig. 5b). The particle size of MnO_2 was investigated from high-resolution TEM images, in which an average diameter of 21.44 ± 1.18 was calculated (Inset of Fig. 4d). To evaluate the electrochemical

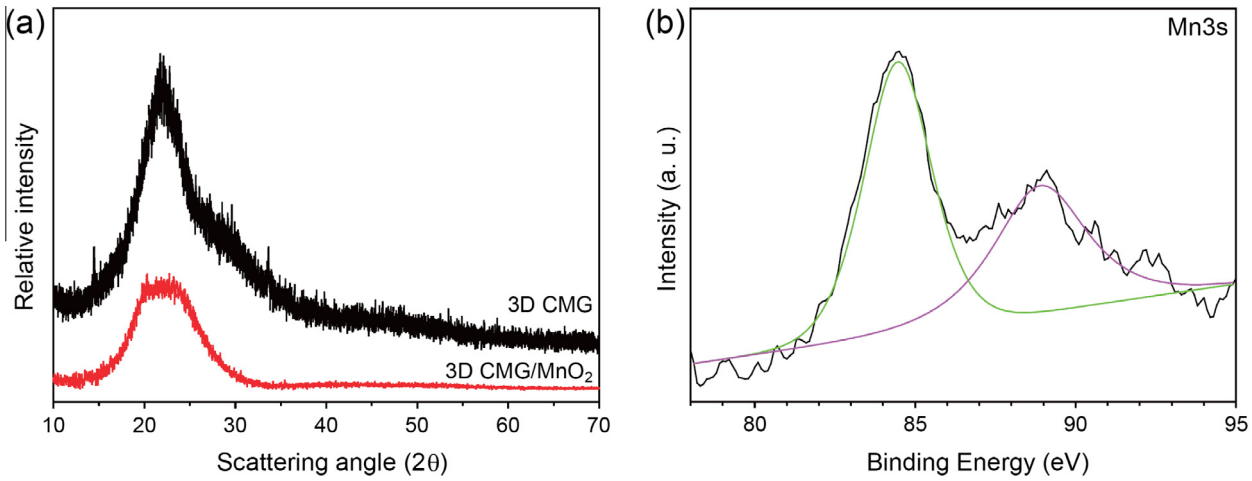

Fig. 5. (a) XRD patterns of 3D CMG and 3D CMG/MnO_2. (b) Mn 3s spectrum of 3D CMG/MnO_2.

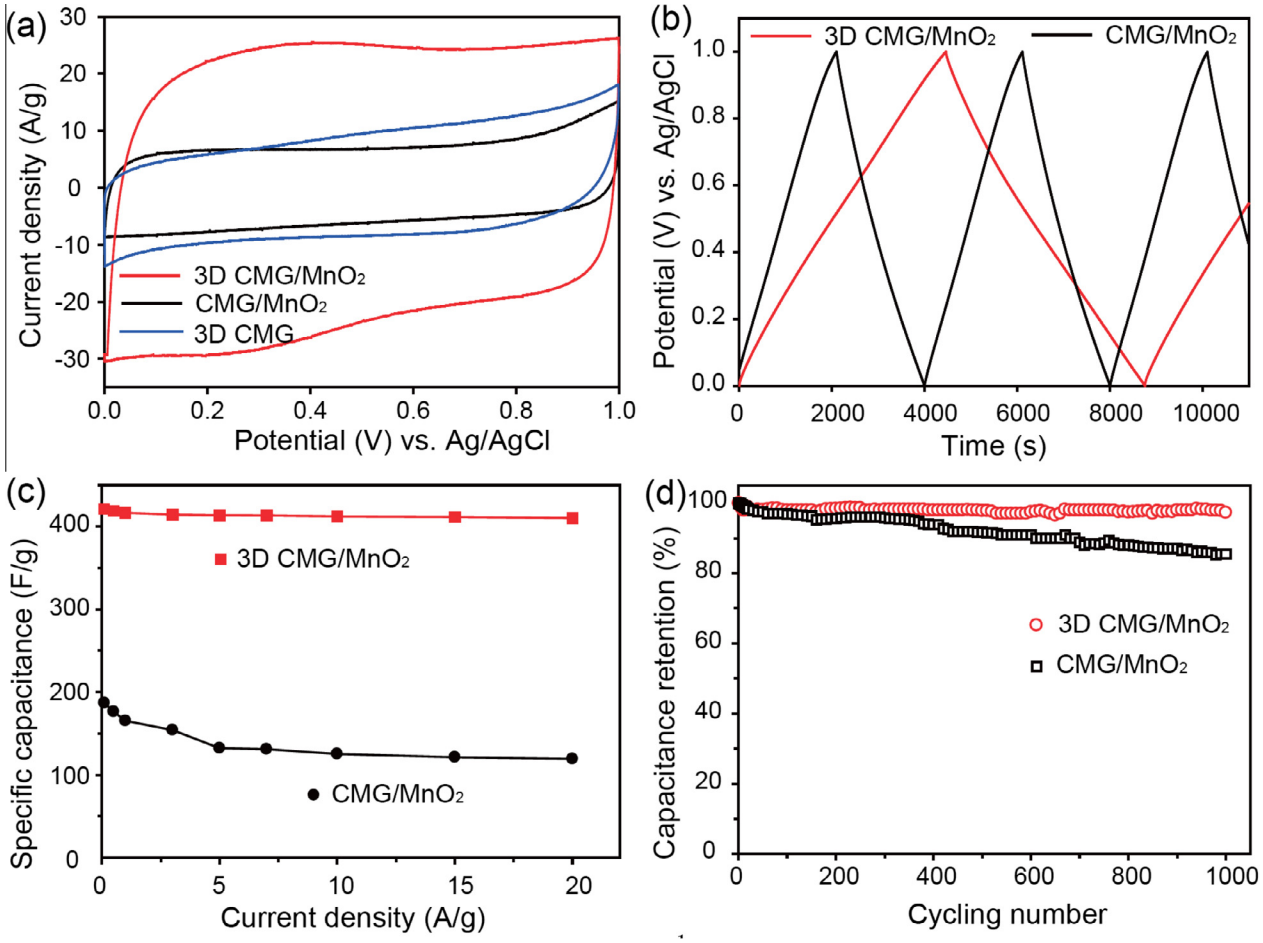

Fig. 6. (a) CV curves with a scan rate of 50 mV s^{-1} for 3D CMG/MnO_2, 3D CMG, and CMG/MnO_2 electrodes in 1 M Na_2SO_4. (b) Galvanostatic charge/discharge curves with a constant current density of 0.1 A g^{-1} for 3D CMG/MnO_2 and CMG/MnO_2 electrodes in 1 M Na_2SO_4. (c) Specific capacitances as a function of current density from 0.1 to 20 A g^{-1} for 3D CMG/MnO_2 and CMG/MnO_2 electrodes. (d) Long-term cycling stability of 3D CMG/MnO_2 and CMG/MnO_2 electrodes with a constant current density of 1 A g^{-1} over 1000 cycling.

characteristics, we carried out cyclic voltammetry (CV), galvanostatic charge/discharge, and electrochemical impedance spectroscopy (EIS) measurements in a three-electrode configuration. The CMG/MnO_2 electrode without PS sphere treatment as a control sample was tested under identical conditions.

CV profiles (Fig. 6a) of the 3D CMG/MnO_2, 3D CMG, and CMG/MnO_2 electrodes were measured at a scanning rate of 50 mV s^{-1} in 1.0 M Na_2SO_4 aqueous solution. The shapes of these CV curves are quasi rectangular which is attributed to the electrical double layer capacitive behavior of CMG and pseudocapacitive behavior of MnO_2 [25]. As expected, higher current density was observed for the 3D CMG/MnO_2 than those of 3D CMG and CMG/MnO_2 counterparts (Fig. 6a). Galvanostatic charge/discharge curves of Fig. 6b also reveal the superior capacitive behavior of 3D CMG/MnO_2 compared to the CMG/MnO_2. High symmetric charge/discharge curves were observed at both samples. These are consistent with the CV curve. On the basis of these curves, the specific capacitance (C_{sp}) of 3D CMG/MnO_2 was calculated to be 421 F g^{-1} at 0.1 A g^{-1}, which is 2 times higher than that of CMG/MnO_2 (187 F g^{-1}). In addition, this specific capacitance value for 3D CMG/MnO_2 is much higher than those of other reported MnO_2-based materials including MnO_2/graphene composite (216 F g^{-1} at 0.15 A g^{-1}) [26], MnO_2/conducting polymer (270 F g^{-1} at 0.25 V s^{-1}) [27], and Au-MnO_2/carbon nanotube (68 F g^{-1} at 6.6 A g^{-1}) [28]. The C_{sp} versus current density was plotted in Fig. 6c. Upon all of the current densities, 3D CMG/MnO_2 yields greatly improved capacitance values with 2–3 times higher than those of CMG/MnO_2. Moreover, the capacitance retention for 3D CMG/MnO_2 was observed to be ~97% when the current rate was increased from 0.1 to 20 A g^{-1}, while 36% capacitance decay was observed for CMG/MnO_2. This indicates the superior rate capability of 3D CMG/MnO_2 compared to the control sample.

To further characterize the electrochemical long-term stability, galvanostatic charge/discharge measurement was performed at a constant current density of 1 A g^{-1} for 1000 cycles. The C_{sp} values as a function of cycle number for 3D CMG/MnO_2 and CMG/MnO_2 were plotted in Fig. 6d. It is seen that 97% of the initial capacitance was retained, indicating good cycling stability of 3D CMG/MnO_2. By contrast, CMG/MnO_2 shows a larger capacitance loss with 85% retention of initial capacitance after 1000 cycles. Nyquist plots were obtained from EIS measurement using 3D CMG/MnO_2 and CMG/MnO_2 electrodes (Fig. 7). The charge transfer resistance (R_{CT}) was calculated to be 14.7 and 22.1 Ω for 3D CMG/MnO_2 and CMG/MnO_2, respectively. Superior charge transfer reaction of 3D CMG/MnO_2 compared to the counterpart was attributed to the increased contact area at the electrolyte/electrode interface [13]. Moreover, a more vertical straight line at the low frequency region for 3D CMG/MnO_2 compared to the CMG/MnO_2 demonstrates the faster ion diffusion behavior, which resulted from porous structures [29]. Therefore, the creation of the porous structure on CMG sheets enabled efficient and rapid pathways for electron and ion transfer, giving rise to a good cycle performance and rate capability.

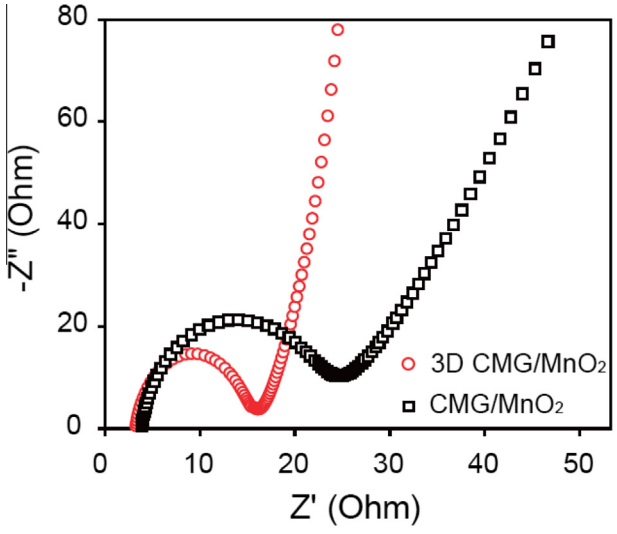

Fig. 7. Nyquist plots measured at a frequency range of 100 kHz to 0.01 Hz for 3D CMG/MnO_2 and CMG/MnO_2 electrodes.

4. Conclusion

We developed a combination method of both replication process and sonochemistry for fabrication of 3D CMG/NP foams. The resulting 3D foams had large surface area and porous structures decorated with various NPs such as Pt, Au, Pd, Ru, and MnO_2. By adapting 3D CMG/MnO_2 into electrode materials, we demonstrated its electrochemical characteristics for supercapacitor applications, showing high specific capacitance, high rate capability, and long cycling life. This promising synthetic method demonstrated here can be generally applicable for the fabrication of various 3D CMG-based foams with other nanoparticles for the development of energy storage and conversion devices as well as electrochemical biosensors.

Acknowledgements

This research was financially supported by the "Electronic medical equipment part & material industrialization foundation construction program" through the Ministry of Trade, Industry & Energy (MOTIE) and Korea Institute for Advancement of Technology (KIAT). This work was also supported by BioNano HealthGuard Research Center funded by the Ministry of Science, ICT & Future Planning (MSIP) of Korea as Global Frontier Project (Grant Number H–GUARD_2013M3A6B2078945).

References

[1] S. Stankovich, D.A. Dikin, R.D. Piner, K.A. Kohlhaas, A. Kleinhammes, Y. Jia, Y. Wu, S.T. Nguyen, R.S. Ruoff, Synthesis of graphene-based nanosheets via chemical reduction of exfoliated graphite oxide, Carbon 45 (2007) 1558–1565.
[2] S. Park, R.S. Ruoff, Chemical methods for the production of graphenes, Nat. Nanotechnol. 4 (2009) 217–224.
[3] B.G. Choi, H.S. Park, T.J. Park, M.H. Ynag, J.S. Kim, S.-Y. Jang, N.S. Heo, S.Y. Lee, J. Kong, W.H. Hong, Solution chemistry of self-assembled graphene nanohybrids for high-performance flexible biosensors, ACS Nano 4 (2010) 2910–2918.
[4] B.G. Choi, J. Hong, W.H. Hong, P.T. Hammond, H. Park, Facilitated ion transport in all-solid state flexible supercapacitors, ACS Nano 5 (2011) 7205–7213.
[5] H. Bai, C. Li, G. Shi, Functional composite materials based on chemically converted graphene, Adv. Mater. 23 (2011) 1089–1115.
[6] J.-Y. Lin, C.-Y. Chan, S.-W. Chou, Electrophoretic deposition of transparent MoS_2-graphene nanosheet composite films as counter electrodes in dye-sensitized solar cells, Chem. Commun. 49 (2013) 1440–1442.
[7] J. Zhang, F. Zhao, Z. Zhang, N. Chen, L. Qu, Dimension-tailored functional graphene structures for energy conversion and storage, Nanoscale 5 (2013) 3112–3126.
[8] L. Yan, Y.B. Zheng, F. Zhao, S. Li, X. Gao, B. Xu, P.S. Weiss, Y. Zhao, Chemistry and physics of a single atomic layer: strategies and challenges for functionalization of graphene and graphene-based materials, Chem. Soc. Rev. 41 (2012) 97–114.
[9] C. Li, G. Shi, Three-dimensional graphene architectures, Nanoscale 4 (2012) 5549–5563.
[10] H. Bai, C. Li, X. Wang, G. Shi, A pH-sensitive graphene oxide composite hydrogel, Chem. Commun. 46 (2010) 2376–2378.
[11] Y. Xu, K. Sheng, C. Li, G. Shi, Self-assembled graphene hydrogel via a one-step hydrothermal process, ACS Nano 4 (2010) 4324–4330.
[12] B.G. Choi, S.-J. Chang, Y.B. Lee, J.S. Bae, H.J. Kim, Y.S. Huh, 3D heterostructured architectures of Co_3O_4 nanoparticles deposited on porous graphene surfaces for high performance of lithium ion batteries, Nanoscale 4 (2012) 5924–5930.
[13] B.G. Choi, M. Yang, W.H. Hong, J.W. Choi, Y.S. Huh, 3D macroporous graphene frameworks for supercapacitors with high energy and power densities, ACS Nano 6 (2012) 4020–4028.

[14] Z. Niu, J. Chen, H.H. Hng, J. Ma, X. Chen, A leavening strategy to prepare reduced graphene oxide foams, Adv. Mater. 24 (2012) 4144–4150.
[15] V. Strong, S. Dubin, M.F. El-Kady, A. Lech, Y. Wang, B.H. Weiller, R.B. Kaner, Patterning and electronic tuning of laser scribed graphene for flexible all-carbon devices, ACS Nano 6 (2012) 1395–1403.
[16] X. Huang, K. Qian, J. Yang, J. Zhang, L. Li, C. Yu, D. Zhao, Functional nanoporous graphene foams with controlled pore sizes, Adv. Mater. 24 (2012) 4419–4423.
[17] R. Liu, J. Duay, S.B. Lee, Heterogeneous nanostructured electrode materials for electrochemical energy storage, Chem. Commun. 47 (2011) 1384–1404.
[18] D. Li, M.B. Müller, S. Gilje, R.B. Kaner, G.G. Wallace, Processable aqueous dispersions of graphene nanosheets, Nat. Nanotechnol. 3 (2008) 101–105.
[19] G. Park, L. Bartolome, K.G. Lee, S.J. Lee, D.H. Kim, T.J. Park, One-step sonochemical synthesis of a graphene oxide-manganese oxide nanocomposite for catalytic glycolysis of poly(ethylene terephthalate), Nanoscale 4 (2012) 3879–3885.
[20] J.H. Bang, K.S. Suslick, Applications of ultrasound to the synthesis of nanostructured materials, Adv. Mater. 22 (2010) 1039–1059.
[21] X. Jin, W. Zhou, S. Zhang, G.Z. Chen, Nanoscale microelectrochemical cells on carbon nanotubes, Small 3 (2007) 1513–1517.
[22] B.G. Choi, M.H. Yang, T.J. Park, Y.S. Huh, S.Y. Lee, W.H. Hong, H. Park, Programmable peptide-directed two dimensional arrays of various nanoparticles on graphene sheets, Nanoscale 3 (2011) 3208–3213.
[23] B.G. Choi, H.S. Park, Controlling size, amount, and crystalline structure of nanoparticles deposited on graphenes for highly efficient energy conversion and storage, ChemSusChem 5 (2012) 709–715.
[24] S.W. Lee, J. Kim, S. Chen, P.T. Hammond, Y. Shao-Horn, Carbon nanotube/manganese oxide ultrathin film electrodes for electrochemical capacitors, ACS Nano 4 (2010) 3889–3896.
[25] Y. Cheng, S. Lu, H. Zhang, C.V. Varanasi, J. Liu, Synergistic effects from graphene and carbon nanotubes enable flexible and robust electrodes for high-performance supercapacitors, Nano Lett. 12 (2012) 4206–4211.
[26] S. Chen, J. Zhu, X. Wu, Q. Han, X. Wang, Graphene oxide–MnO_2 nanocomposites for supercapacitors, ACS Nano 4 (2010) 2822–2830.
[27] R. Liu, J. Duay, S.B. Lee, Electrochemical formation mechanism for the controlled synthesis of heterogeneous MnO_2/Poly(3,4-ethylenedioxythiophene) nanowires, ACS Nano 5 (2011) 5608–5619.
[28] A.L.M. Reddy, M.M. Shaijumon, S.R. Gowda, P.M. Ajayan, Multisegmented Au-MnO_2/carbon nanotube hybrid coaxial arrays for high-power supercapacitor applications, J. Phys. Chem. C 114 (2010) 658–663.
[29] M. Hughes, G.Z. Chen, M.S.P. Shaffer, D.J. Fray, A.H. Windle, Electrochemical capacitance of a nanoporous composite of carbon nanotubes and polypyrrole, Chem. Mater. 14 (2002) 1610–1613.